Computational methods for Generalized Sturmians basis

Darío M. Mitnik [a,b,e,*], Flavio D. Colavecchia [c,e], Gustavo Gasaneo [d,e], Juan M. Randazzo [c,e]

[a] *Departamento de Física, FCEyN, Universidad de Buenos Aires, Argentina*
[b] *Instituto de Astronomía y Física del Espacio (IAFE), C.C. 67, Suc. 28, (C1428EGA) Buenos Aires, Argentina*
[c] *Centro Atómico Bariloche, 8400 Bariloche, Río Negro, Argentina*
[d] *Departamento de Física, Universidad Nacional del Sur, 8000 Bahía Blanca, Buenos Aires, Argentina*
[e] *Consejo Nacional de Investigaciones Científicas y Técnicas (CONICET), Argentina*

ARTICLE INFO

ABSTRACT

The computational techniques needed to generate a two-body Generalized Sturmian basis are described. These basis are obtained as a solution of the Schrödinger equation, with two-point boundary conditions. This equation includes two central potentials: A general auxiliary potential and a short-range generating potential. The auxiliary potential is, in general, long-range and it determines the asymptotic behavior of all the basis elements. The short-range generating potential rules the dynamics of the inner region. The energy is considered a fixed parameter, while the eigenvalues are the generalized charges. Although the finite differences scheme leads to a generalized eigenvalue matrix system, it cannot be solved by standard computational linear algebra packages. Therefore, we developed computational routines to calculate the basis with high accuracy and low computational time. The precise charge eigenvalues with more than 12 significant figures along with the corresponding wave functions can be computed on a single processor within seconds.

© 2011 Elsevier B.V. All rights reserved.

1. Introduction

Sturmian functions were introduced by Shull and Löwdin [1] as a complete basis set to deal with atomic systems. Later Rotenberg [2,3] gave them the name *Sturmian* to emphasize their connection with the Sturm–Liouville theory. Glöckle and co-workers used Weinberg states (which are actually Sturmian functions) in scattering problems [4]. In 1968, Goscinski [5] presented a rigorous mathematical generalization of this basis set. He regarded Sturmians as solutions to the Schrödinger equation with a constant and externally defined energy, and considered the magnitude of the potential (the "charges") as the eigenvalues [5,6].

The advantages of the Sturmian functions are considerable, especially comparing their efficiency as a basis set with the hydrogenic eigenvectors of the Schrödinger equation. The functions constituting a Sturmian basis set are thickly crowded on a spatial region. That region can be adjusted to be the desired region of interest through the adequate choice of the energy parameter. The peculiarity of the bound-state hydrogenic wave functions, on the other hand, is that the innermost zeros of the functions are insensitive to the principal quantum number n. This accounts for the fact that these functions do not form a complete set; the continuum is required to describe the region between the origin and the limiting first zero. The bound-hydrogenic functions are also widely spread in space, because the maximum value position behaves proportional to n^2.

Negative energy Sturmian functions, which asymptotically decrease exponentially, were shown to be efficient in obtaining atomic bound states for few-electron atoms as well as in molecular systems. These functions have been widely used to perform *ab initio* calculations of N-electron atomic and molecular systems (see, for example, [7] and references within). Their use improves substantially the convergence of the expansion for many configuration–interaction calculations, as shown, for instance, in [1, 8,9].

Positive energy Sturmians, on the other hand, can be potentially useful for scattering problems, because one can generate functions having the same energy as the physical scattering particle (the same wavenumber) and the same asymptotic boundary. For example, all the functions in a Sturmian basis set can have outgoing—or incoming—wave conditions. However, the positive Sturmian functions form a continuum basis set with an infinite and continuum spectrum [10,11]. Even though a finite basis size can be developed such that the spectrum discretizes, regularization of the wavefunctions often leads to potentially divergent functions, unless the energy itself becomes complex. This make them impractical to be used on scattering problems.

Complex energy Sturmian function can be obtained by performing a complex scaling rotation. As an example of applications of complex-rotated positive energy Sturmian functions in scatter-

* Corresponding author at: Instituto de Astronomía y Física del Espacio (IAFE), C.C. 67, Suc. 28, (C1428EGA) Buenos Aires, Argentina.
E-mail address: dmitnik@df.uba.ar (D.M. Mitnik).

ing problems, we can mention the works performed by the Piraux group using the J-matrix method. They have been employing these functions within time-independent and time-dependent approaches to solve the Schrödinger equation in calculations of single and double photoionization of He [12] as well as ionization-excitation of neutral atoms [13].

The Sturmian functions obtained as discrete solutions of the Schrödinger equation with a pure Coulomb interaction are called Coulomb Sturmian functions (CSF). These are by far the most widely used Sturmian functions, to such an extent that this is the only kind of functions employed in all the papers cited up to this point. Basis sets obtained for general potential are very scarce because there are only a few two-body potentials that admit closed-form analytical solutions. Some examples of them were discussed by Rawitscher [14], and by Macek and Ovchinnikov [15,16].

Our purpose is to generate a discrete set of wavefunctions having a unique behavior at large distances. The set should have only asymptotically outgoing (or incoming) waves, all with the same wave number corresponding to the physical scattering energy. We also require the functions to be regular at the origin, and to differ from each other by the number of nodes within the inner region. However, energy is not the only parameter that determines the asymptotic behavior of the wavefunctions. One can impose an outgoing behavior to the CSF basis set, but since each one of these basis elements belongs to a different charge eigenvalue, their individual asymptotic behavior is different.

In an attempt to generalize the use of Sturmian basis functions, we introduced Generalized Sturmian functions (GSF) (see, for example, [14,17,18]), in which two potentials are included into the Schrödinger equation. One potential—called the *auxiliary potential*—is, in general, a long-range one that determines the asymptotic behavior of all the basis set. The other is a short-range potential—called the *generating potential*—which accounts for the dynamics of the inner region, where the two particles interact strongly with each other.

Examples of the application of GSF for accurate three-body systems calculations, and the usefulness of this basis in scattering problems are thoroughly presented in Randazzo's PhD thesis [19], and are also well illustrated in other papers published by our group. It is beyond the scope of the present work to discuss these cases.

The only paper that provides a systematic way of obtaining a GSF basis [14] discusses the case of a Woods–Saxon potential, checking the numerical procedure for the limit of a square well potential for which the continuum functions and the corresponding eigenvalues are known.

We found many difficulties at the initial stage of our research, particularly in the GSF generation. Although the GSF bases offers many advantages, they were not used extensively, possibly because of those very difficulties. We present here a general computational method for generating the GSF basis set, for any combination of auxiliary and generating potentials. The impracticability of the calculations, the scarcity of appropriate literature and the lack of public available subroutines needed in the computation, have led us to present the numerical details and technicalities, to explain the routines used, and to make public our own computational programs.

2. General theory of Sturmian basis

The Generalized Sturmian radial functions are the solutions of the Schrödinger equation (in atomic units):

$$\left[-\frac{1}{2}\frac{d^2}{dr^2} + \frac{l(l+1)}{2r^2} + U(r) - E \right] S_{nl}(r) = -\beta_{nl} V(r) S_{nl}(r) \qquad (1)$$

where $U(r)$ is the auxiliary potential (e.g. Coulomb), and $V(r)$ is the short-range generating potential, which vanishes in the outer region $r > R_S$. In contrast to the traditional time-independent Schrödinger equation, where the charge is fixed and its solution leads to the energy eigenvalues, in Eq. (1) the energy E is a fixed parameter, and the charges become the eigenvalues β_{nl}. Besides, two boundary conditions supplement the equation. In every case along the paper, we are seeking for solutions having a regular boundary condition at the origin

$$S_{nl}(r = 0) = 0. \qquad (2)$$

If the auxiliary potential $U(r)$ is a Coulomb potential, then, in addition, the Kato cusp condition should also be imposed, as discussed in [20].

In the outer region, where the second boundary condition is imposed, the auxiliary potential vanishes. The solutions of this Sturmian equation represent a particle of energy E moving under the influence of a potential $U(r)$. The radial Sturmian equation (1) reduces to

$$\left[-\frac{1}{2}\frac{d^2}{dr^2} + \frac{l(l+1)}{2r^2} + U(r) - E \right] S_{nl}(r) = 0 \quad \text{for } r > R_S. \qquad (3)$$

The solutions $S_{nl}(r)$ will present all the same asymptotic behavior, that is, the asymptotic equation does not involve the eigenvalue.

Eq. (1) together with the boundary conditions (2) and (3), define a Sturm–Liouville problem. Therefore, their solutions conform a complete basis set, obeying a potential-weighted orthogonality relation:

$$\int_0^\infty S_{n'l}(r) V(r) S_{nl}(r)\, dr = 0 \quad \text{for } n' \neq n. \qquad (4)$$

Two important issues should be noticed related to this orthogonality relation. The first is that due to the fact that the generating potential $V(r)$ is of short-range, the integration (4) can be performed numerically in a finite spatial region for any value of the energy E, without any additional special requirement over the $S_{nl}(r)$ functions. The second issue to notice is that the integral is defined without taking the complex conjugate of the function $S_{n'l}(r)$. Under this particular choice of the scalar product, the overlaps between the functions converged for any energies and potentials.

Let us now illustrate that the $S_{nl}(r)$ functions have the same asymptotic behavior, with different examples, beginning with the case of negative energies $E < 0$. For a short-range auxiliary potential $U(r)$ (i.e., $U(r)$ also vanishes in the outer region) the asymptotic solutions of (3) behave like

$$\lim_{r \to \infty} S_{nl} \propto e^{-\kappa r}, \qquad (5)$$

where $\kappa = \sqrt{-2E}$. Since E is a fixed parameter, all the basis functions have the same asymptotic behavior.

In the case of a Coulombic auxiliary potential $U(r) = -Z/r$, the solutions of (1) have an asymptotic condition consisting of an exponentially decaying factor $\exp(-\kappa r)$ multiplied by a logarithmic factor

$$\lim_{r \to \infty} S_{nl} \propto e^{-\kappa r + \frac{Z}{\kappa}\ln(2\kappa r)}, \qquad (6)$$

which is the same for all basis elements.

At this point we would like to emphasize the difference between our Generalized Sturmian functions with the Coulombic auxiliary potential, and the Coulomb Sturmian functions. The CSF are solutions of

$$\left[-\frac{1}{2}\frac{d^2}{dr^2} + \frac{l(l+1)}{2r^2} - E\right]S_{C_{nl}}(r) = \beta_{nl}\frac{1}{r}S_{C_{nl}}(r), \qquad (7)$$

i.e., the same Eq. (1) with $U(r) = 0$ and $V(r) = -1/r$. The discretized character of the solutions imposes $\beta_{nl} = n\kappa$. In this case, the asymptotic behavior of the CSF is

$$\lim_{r\to\infty} S_{C_{nl}} \propto e^{-\kappa r + n\ln(2\kappa r)} = (2\kappa r)^n e^{-\kappa r} \qquad (8)$$

which changes from one CSF element to another, due to the presence of the factor n.

For the cases in which the energy is positive, the free auxiliary potential ($U(r) = 0$) produces the following asymptotic conditions. For a short-range generating potential ($V(r) = 0$ for $r > R_S$),

$$\lim_{r\to\infty} S_{nl} \propto e^{\pm ikr}, \qquad (9)$$

where $k = \sqrt{2E}$ and the sign describes outgoing $(+)$ or incoming $(-)$ waves. The Coulomb case ($V(r) = -Z/r$) produces functions with the asymptotic condition

$$\lim_{r\to\infty} S_{nl} \propto e^{\pm i(kr + \frac{Z_n}{k}\ln(2kr))}, \qquad (10)$$

where $Z_n = \beta_n Z$. All the functions oscillate with the same wavenumber k (determined externally by the fixed energy), but each of them has a different logarithmic phase, depending on the eigenvalue. For the CSF, the charge Z_n is complex, and Eq. (10) leads to divergent wavefunctions, except for particular cases in which the parameter k is also complex. Introducing complex energies becomes a procedure similar to the complex-rotation method, in the sense that the outgoing functions vanish asymptotically. However, these two methods are not equivalent. Issues like the relationship between complex-rotation of the coordinate and the energy, and Generalized Sturmian set obtained with complex rotated coordinate, are subject of current investigations [21]. As far as we know, Generalized Sturmian functions for complex energies do not exist in the scientific literature.

3. Numerical methods

3.1. Finite differences scheme

We solve Eq. (1) by using a finite differences scheme. To this aim, we first discretize the solution $S_{nl}(r)$:

$$S_{nl}(r_i) \equiv S_i, \quad i = 1\ldots N, \qquad (11)$$

in the uniform radial grid $r_i = i \times \Delta r$ (the quantum numbers l and n are suppressed for brevity). The functions S_i are then defined up to a given radius $R = N \times \Delta r$. Within the finite difference scheme, we can approximate the second order derivative in Eq. (1) up to $O(\Delta r^2)$ by:

$$\frac{d^2 S_{nl}(r_i)}{dr^2} = \frac{1}{\Delta r^2}[S_{i+1} - 2S_i + S_{i-1}] + O(\Delta r^2). \qquad (12)$$

Therefore, in this three-point stencil, Eq. (1) reads:

$$-\frac{1}{2}\frac{1}{\Delta r^2}S_{i+1} - \frac{1}{2}\frac{1}{\Delta r^2}S_{i-1} + \left[\frac{1}{\Delta r^2} + \frac{l(l+1)}{2\Delta r^2 i^2} + U_i - E\right]S_i$$
$$= -\beta V_i S_i + O(\Delta r^2), \qquad (13)$$

where $V_i \equiv V(r_i)$ and $U_i \equiv U(r_i)$. We write this finite recurrence relation in matrix form as

$$[\mathbf{H} - E\mathbf{I}]\mathbf{s} = -\beta\mathbf{V}\mathbf{s}, \qquad (14)$$

where $\mathbf{s}$ is the vector with elements S_i, $\mathbf{I}$ is the identity matrix, and $\mathbf{V}$ is the diagonal matrix with elements $\mathbf{V}_{ii} = V_i$. The symmetric tridiagonal matrix $\mathbf{H}$ has off-diagonal elements

$$\mathbf{H}_{i,i-1} = \mathbf{H}_{i,i+1} = -\frac{1}{2}\frac{1}{\Delta r^2}, \qquad (15)$$

while the diagonal ones are

$$\mathbf{H}_{ii} \equiv h_i = \frac{1}{\Delta r^2} + \frac{l(l+1)}{2\Delta r^2 i^2} + U_i. \qquad (16)$$

The boundary condition given by Eq. (2) is naturally fulfilled by the functions, since the grid starts at $i = 1$, and that means $S_0 = 0$. Within this scheme, we are also able to set the boundary conditions for the outer part of the functions, by choosing the appropriate values of $\mathbf{H}_{N,N}$, the last diagonal element in Eq. (16). For example, box boundary conditions, which means that the function $S(r) = 0$ for $r > R$, can simple be imposed to the system, without any change of the diagonal elements. For any other asymptotic behavior, the last diagonal element of the matrix $\mathbf{H}$ is modified assuming that this asymptotic condition was already reached at $r_i = R$. Defining

$$C_N \equiv \frac{S_{N+1}}{S_N} \qquad (17)$$

then, the first term in the LHS of Eq. (13) becomes, for the last matrix element

$$-\frac{1}{2}\frac{1}{\Delta r^2}S_{N+1} = -\frac{1}{2}\frac{1}{\Delta r^2}S_N C_N. \qquad (18)$$

Thus, an approximate solution with the exact boundary condition can be obtained from Eq. (13) making the substitution:

$$h_N \to h_N - \frac{1}{2}\frac{1}{\Delta r^2}S_N C_N. \qquad (19)$$

For example, if the Coulombian outgoing asymptotic boundary condition (10) is desired, then

$$C_N = \frac{S_{N+1}}{S_N} = \frac{e^{i(kr_{N+1} + \frac{Z}{k}\ln(2kr_{N+1}))}}{e^{i(kr_N + \frac{Z}{k}\ln(2kr_N))}} = e^{i(k\Delta r + \frac{Z}{k}\ln(2k\Delta r))}. \qquad (20)$$

In previous works [17,18,20,22] we tested the quality of the configuration–interaction method based on the GSF basis. There, we aimed to obtain the eigenfunctions with high accuracy. Therefore, a finite difference scheme of the order $O(\Delta r^4)$, leading to a pentadiagonal matrix eigenvalue problem, was used. In general, increasing the order or the approximation used for the spatial derivatives is very efficient since it produces eigenvalues with much higher accuracy, with a small computational increase of the computational time [19].

3.2. Eigenvalues calculation by standard diagonalization routines

Eq. (14) is a generalized eigenvalues problem, and in principle, it should be solved by standard computational linear algebra routines like for example, the subroutine ZGGEVX from LAPACK [23]. Unfortunately, this procedure does not work. We implemented the LAPACK subroutines in our codes—obtaining wrong eigenvalues and eigenvectors—for many different combinations of auxiliary and generating potentials. Perhaps the reason of this failure lies in the short-range character of the right side of the generating potential $V(r)$. The size of the matrix in Eq. (14) should be large enough for the auxiliary potential $U(r)$ to vanish smoothly, and to ensure that the boundary conditions are already fulfilled at the last element of the matrix. Otherwise, Eq. (17) will not accurately represent the desired asymptotic behavior. But, extending the matrices to large distances means that many elements in the right side of Eq. (14) are zeroes, making the calculations unstable.

Since the generalized eigenvalues solver did not work, we also tried the use of the standard subroutines for the eigenvalues solver. In order to do that, we multiplied both sides of Eq. (14) by the

inverse of the diagonal potential matrix (i.e. by $\mathbf{V}^{-1}$), obtaining the eigensystem:

$$\mathbf{V}^{-1}[\mathbf{H} - E\mathbf{I}]\mathbf{s} = -\beta\mathbf{s}. \tag{21}$$

The three-point stencil for this equation is:

$$-\frac{1}{2}\frac{1}{\Delta r^2 \overline{V}_{i+1}}S_{i+1} - \frac{1}{2}\frac{1}{\Delta r^2 \overline{V}_{i-1}}S_{i-1}$$

$$+ \left[\frac{1}{\Delta r^2} + \frac{l(l+1)}{2\Delta r^2 i^2} + U_i - E\right]\frac{1}{V_i}S_i$$

$$= -\beta S_i + O(\Delta r^2), \tag{22}$$

where

$$\overline{V}_{i\pm1} \equiv \sqrt{V_i V_{i\pm1}} \tag{23}$$

was introduced in order to keep the symmetry of the matrix.

The presence of $\mathbf{V}^{-1}$ in the diagonal elements of the matrix makes the eigensystem very unstable, and requires that we restrict the numerical calculation to a region in which the potential $V(r)$ is not too small. There is an additional problem associated with the use of standard diagonalization routines, and it relates to the computational requirements. For an acceptable accuracy, sometimes several thousand points are required in the spatial discretization. Although the matrix is banded, an enormous memory space must be allocated for storing the eigenvalues, as required in most of the LAPACK routines. For scattering solutions, the replacement of the last matrix element in Eq. (19) leads to a non-Hermitian tridiagonal matrix, a case for which there are not public routines available.

For those reasons, we had to develop our own computational routines, presented in detail in the following subsections.

3.3. Eigenvalues calculation by a complex-orthogonal transformation

A fast and accurate algorithm for solving the tri-diagonal eigenvalue problem (22) based on the theory explained by Luk and Qiao [24] was implemented. We used the implicit QR method with the Wilkinson shift [25] and replaced all unitary transformations by complex-orthogonal transformations. The theoretical aspects of the algorithm are discussed in that paper, and in the references therein. However, they present a simple case of a 4×4 matrix, without any guarantee that the algorithm will be appropriate for large systems. Moreover, since we made several modifications to the procedure outlined there, we consider it necessary to provide the details of the computational techniques implemented by us.

Basically, the diagonalization algorithm consists of performing successive transformations of the form

$$\mathbf{A}^{(j+1)} = \mathbf{W}^{(j)}\mathbf{A}^{(j)}(\mathbf{W}^{(j)})^T, \tag{24}$$

to a complex-symmetric tri-diagonal matrix $\mathbf{A}$ at any step j, where $\mathbf{A}^{(1)} = \mathbf{A}$, $\mathbf{W}^{(j)}$ are complex-orthogonal matrices

$$\mathbf{W}^{(1)} = \begin{pmatrix} c_1 & s_1 & 0 & 0 & \cdots & 0 & 0 \\ -s_1 & c_1 & 0 & 0 & \cdots & 0 & 0 \\ 0 & 0 & 1 & 0 & \cdots & 0 & 0 \\ \cdots & \cdots & \cdots & \cdots & \cdots & \cdots & \cdots \\ 0 & 0 & 0 & \cdots & 0 & 0 & 1 \end{pmatrix};$$

$$\mathbf{W}^{(2)} = \begin{pmatrix} 1 & 0 & 0 & 0 & \cdots & 0 & 0 \\ 0 & c_2 & s_2 & 0 & 0 & \cdots & 0 \\ 0 & -s_2 & c_2 & 0 & 0 & \cdots & 0 \\ \cdots & \cdots & \cdots & \cdots & \cdots & \cdots & \cdots \\ 0 & 0 & 0 & \cdots & 0 & 0 & 1 \end{pmatrix};$$

$$\vdots$$

$$\mathbf{W}^{(N-1)} = \begin{pmatrix} 1 & 0 & 0 & 0 & \cdots & 0 & 0 \\ 0 & 1 & 0 & 0 & 0 & \cdots & 0 \\ \cdots & \cdots & \cdots & \cdots & \cdots & \cdots & \cdots \\ 0 & 0 & 0 & 0 & 0 & c_N & s_N \\ 0 & 0 & 0 & 0 & 0 & -s_N & c_N \end{pmatrix}, \tag{25}$$

and the coefficients c_i and s_i are chosen appropriately in order to annihilate the non-diagonal terms of the matrix $\mathbf{A}$. Due to the particular form of the rotation matrices $\mathbf{W}$, it is not necessary to perform the multiplication (24) for the full $N \times N$ matrix. It is possible to perform the transformations with reduced 2×2 matrices

$$\mathbf{G}^{(j)} = \begin{pmatrix} c_j & s_j \\ -s_j & c_j \end{pmatrix}, \tag{26}$$

as is explained in detail in Appendix A.

The $(N-1)$ transformations (24) are repeated many times (usually, about ten times for each eigenvalue) until the off-diagonal element annihilates, or becomes smaller than some convergence criterion, which in our case is set at

$$|A_{i+1,i}| \leqslant \sqrt{2}(|A_{i,i}| + |A_{i+1,i+1}|)\epsilon_M, \tag{27}$$

where ϵ_M is the machine precision.

It is worth noting that the computational procedures described in Appendix A not follow exactly the algorithm outlined in [24]. Another point to underline refers to the order in which the eigenvalues are obtained. The algorithm described here does not produce the eigenvalues in an established order. However, throughout the successive iterations they appear in groups of eigenvalues that follow a certain order within the group (this is not strict and we do not fully understand the reason for that). This order is related to the magnitude of the generating potential V. In general, the tendency is for the higher eigenvalues to pop up first, if the potential $V(r)$ decreases with r (i.e., with the index of the matrix). Therefore, we found it more effective to invert the order of the matrix elements, in such a way that $r_1 = N \times \Delta r$, $r_2 = (N-1) \times \Delta r, \ldots,$ $r_N = \Delta r$.

3.4. Eigenvectors calculation

The QR algorithm presented in [24] is able, in principle, to produce also the eigenvectors. The usual form is to produce the same transformations done to the tri-diagonal matrix, to a unit matrix, that at the end of the procedure, will contain, in its columns, the different eigenvectors.

In previous work [17,18] we used a different approach, consisting of the relaxation of a random vector, until it converges to the desired eigenvalue of the matrix $\mathbf{A}$. The random vector $\mathbf{r}$ is successively multiplied, by

$$\mathbf{r} \leftarrow [(\mathbf{A} - \lambda_j\mathbf{1})]^{-1}\mathbf{r}, \tag{28}$$

where λ_j is the eigenvalue for which the corresponding eigenvector is sought. These iterations converge to the eigenvector corresponding to the eigenvalue closer to λ_j. The actual eigenvalue is calculated, and it replaces the original λ_j. We repeat the operation until the change in the eigenvalue is smaller than a particular tolerance. The advantage of this procedure is that it adapts easily to a simple replacement in the degree of approximation of the spatial derivatives, allowing the calculation of the eigenvalues with higher accuracy (for example, by using a five-point stencil in Eq. (21)). Details of the general inversion algorithm are given in [26], and for the particular implementation in the generation of the GSF basis, in [19]).

In the present work, we developed another iterative algorithm that allows to obtain, very fast, very accurate eigenvalues. For any eigenvalue, the corresponding eigenvector is computed by using

a predictor–corrector method. The procedure includes a numerical (outwards) integration from the origin to a particular matching point, and another integration (inwards) from the asymptotic region to the matching point. At this particular matching point the logarithmic derivatives are calculated for both solutions, and iterations are performed until the difference between both values becomes negligible. The full procedure is explained in the following sections.

3.5. Iterative solution of the Sturmian equation

We use finite difference techniques to find the numerical solutions $S_n(r)$ for $n = 1 \ldots N$ to the radial equation (1). For simplicity, we drop the index l corresponding to the angular quantum number here and in the following. We solve the equation on a finite grid covering the region $r = 0$ to a boundary $r = R$, where the boundary conditions are assumed to be applicable. We can choose to calculate the desired regular solution ($S_n(0) = 0$) by starting the numerical integration with the appropriate functional form $S_n(r \to 0) = r^{l+1}$. However, numerical errors near the origin introduce small admixtures of the irregular solution into the solution being sought. Integrating outward from the origin can amplify the errors, producing a divergent function. Therefore, we also start an inward numerical integration, from a *practical infinity* r_∞ located in the asymptotic region, toward the origin. That insures that errors from the small admixtures of the irregular function decrease as the integration proceeds from point to point.

The numerical method used for the solution integration is explained in detail in W. Johnson's book [27]. It consists of a predictor–corrector Adams–Moulton method for the integration. We use a seven-point scheme, which (together with the interpolation procedure) achieves a high order of accuracy (of about $(\Delta r)^8$). The same procedure is implemented for the inward integration. We modified the Johnson's subroutines OUTSCH and INSCH, allowing their use with complex functions.

The procedure is completed with a matching process, which consists of equating the logarithmic derivatives η_n of the outward function S_n^{out} and of the inward function S_n^{inw} at the boundary point $r = R$, i.e.,

$$\eta_n^{\text{out}} = \eta_n^{\text{inw}}, \tag{29}$$

where

$$\eta_n^{\text{out}} \equiv \frac{1}{S_n^{\text{out}}} \frac{\partial S_n^{\text{out}}}{\partial r} \bigg|_{r=R} \tag{30}$$

and

$$\eta_n^{\text{inw}} \equiv \frac{1}{S_n^{\text{inw}}} \frac{\partial S_n^{\text{inw}}}{\partial r} \bigg|_{r=R}. \tag{31}$$

If the absolute value of the discrepancy

$$\Delta \eta_n = \eta_n^{\text{inw}} - \eta_n^{\text{out}} \tag{32}$$

between the two derivatives is higher than a desired parameter, we change the eigenvalue (according to a particular recipe explained below), and iterate until the convergence is achieved. The matching procedure varies according to the particular boundary condition desired, so we will deal separately with the different cases. Without loss of generality, we will assume that the auxiliary potential is asymptotically a Coulombic potential, of the form

$$\lim_{r \to \infty} U(r) = -\frac{Z}{r}. \tag{33}$$

3.5.1. Bound levels

The solutions $S_n(r)$ of Eq. (1) with an auxiliary potential (33) and negative energy E, which are not exponentially divergent, have the asymptotic behavior given in Eq. (6). If the charge $Z \in \mathbb{R}$, the asymptotic behavior is also real, and therefore, the radial flux will be zero: these are stationary eigenvectors. The eigenvalue spectrum in this case is discrete and infinite.

The outward integration starts with an expansion of the solution, assuming that $S_n(r \to 0) = r^{l+1}$. The particular point-by-point scheme used in the propagation of the solution is not crucial, but if accuracy is needed, it must be a high-order scheme. The integration is continued toward the outer classical turning point. Assuming that at this point the generating potential is null (which is a reasonable assumption, since it is a short-range potential), the turning point r_t is obtained by calculating the point in which

$$U(r_t) + \frac{l(l+1)}{2r_t^2} + \beta_n V(r_t) = E \tag{34}$$

is satisfied.

In the region beyond the classical turning point, the equation is integrated inward, again using a point-by-point integration scheme, starting from a *practical infinity* r_∞, with an approximate solution obtained from an asymptotic series. Since a bound state function behaves asymptotically as $e^{-\kappa r}$, we choose the value of r_∞ in such a way that

$$\kappa r_\infty = \sqrt{-2(E - U(r_\infty))} \, r_\infty \approx 40. \tag{35}$$

By choosing that, we ensure that the function has already reached the exponentially decreasing boundary condition, and we are still in a position to avoid numerical problems in the integration. The value of the function $S_n(r_\infty)$ is roughly 10^{-12} of its maximum.

In order to start the propagations (both the outward and the inward propagation), an initial eigenvalue β_n is estimated. We use as the initial value, the eigenvalue given by the algorithm introduced in Section 3.3. The following steps for the iteration are

1. Use the outward integration routine to obtain values of the radial wave function S_n^{out} from the origin to r_∞, and normalized it according to

$$\int_0^\infty S_n^{\text{out}} V(r) S_n^{\text{out}} \, dr = 1. \tag{36}$$

Since $V(r)$ is a short range potential, the upper limit of the integration should be replaced by the point where the potential vanishes.

2. Check the number of nodes of the solution. It must be $(n - l - 1)$, otherwise, change the eigenvalue by roughly a 10% and start the iteration again.
3. Calculate the turning point (Eq. (34)).
4. Use the inward integration routine to calculate the radial wavefunction S_n^{inw} from r_∞ to r_t. Scale the inward solution in order to make the wavefunction continuous, i.e., $S_n^{\text{inw}}(r_t) = S_n^{\text{out}}(r_t)$.
5. Calculate the correction $\Delta \beta_n$ determined by the difference between the slopes of the two curves in the matching point r_t, as given in Eq. (B.10) of Appendix B.
6. Convergence check: The process is repeated until the two curves meet with the same derivative.

In general, only a few iterations are needed for any eigenvector, depending on the quality of the initial eigenvalue given by the tridiagonalization, and the accuracy desired in the final results. We will discuss detailed results in Section 4.

3.5.2. Continuum levels with outgoing/incoming boundary conditions

The first step here is the calculation of the asymptotic wavefunction, providing the auxiliary potential and the initial eigenvalue (which, again, is obtained from the tridiagonalization explained above). For the Coulomb potential, we use the FCOUL routine written by Salvat [28], which provides the regular and irregular radial Schrödinger Coulomb functions $F(\frac{Z}{k}, r)$ and $G(\frac{Z}{k}, r)$, and their derivatives, where $\frac{Z}{k}$ is the Sommerfeld parameter. Since in our calculation the energy is a fixed parameter, we will drop the indexes related to Z or k in the following formulas.

The asymptotic solution is written—in terms of the Coulomb functions—as

$$P(r \geqslant R_A) = \cos\delta F(r) + \sin\delta G(r), \qquad (37)$$

where δ is the phase shift, which is calculated by assuming arbitrarily that at the point R_A the function satisfies $S_n(R_A) = 1$, i.e.:

$$\cos\delta = \frac{F(R_A) + iG(R_A)}{F(R_A)^2 + G(R_A)^2},$$
$$\sin\delta = \frac{G(R_A) - iF(R_A)}{F(R_A)^2 + G(R_A)^2}. \qquad (38)$$

The asymptotic point is initially set as $R_A = N \times \Delta r = R$ (see Eq. (11) and the following definitions). This is the point at which the boundary condition was set in the initial tridiagonalization. Since the auxiliary potential cannot be strictly zero at this point, we allow our program to calculate the wavelength λ of the continuum function (37) and set $R_A = R + 4\lambda$. In any case, we must ensure that $R_A > R_S$, where R_S is the range of the generating potential $V(r)$. The matching point is set as $R_M = R_A/2$.

The rest of the algorithm is similar to that described in the previous section for bound levels. Using the initial eigenvalue, we start the outward integration towards the matching point, and scale the solution in order to obtain $S_n^{out}(R_M) = S_n^{inw}(R_M)$. It must be pointed out that the inward integration is performed for the full Generalized Sturmian radial equation (1), which includes both auxiliary and generating potentials. The inward integration starts at R_A with the assumption of a purely Coulomb function (37), but as the integration propagates inward, the short-range potential modifies that behavior.

In the same way as for the bound levels, the degree of mismatch of the solutions at the matching point allows to estimate the change $\Delta\beta_n$ (using Eq. (B.10)) needed for the next iteration step, until convergence is achieved in the slopes of the outward and inward functions.

3.5.3. Continuum levels with stationary boundary conditions

Although the general algorithm for obtaining the eigenvalues is similar to the previous cases, there are some technicalities that deserve a special mention.

The first step calculates the appropriate phase shift that satisfies, at $R = N \times \Delta r$:

$$S_n(R) = \cos\delta F(R) + \sin\delta G(R) = 0. \qquad (39)$$

The solution is

$$\sin\delta = \frac{1}{1 + (\frac{G(R)}{F(R)})^2},$$
$$\cos\delta = -\sin\delta \frac{G(R)}{F(R)}. \qquad (40)$$

Since the condition $S_n(R) = 0$ is required, there are some numerical difficulties to deal with in this special case. First, it is not possible to match the logarithmic derivative at the point $r = R$. Then, we start the iterations by matching the outward and inward

solutions at a nearby point $R_M = R + \lambda/8$ (we want to avoid the possibility that either the real or the imaginary part of the solution vanishes). The following procedure is the same as outlined for the bound and stationary cases.

We found that the matching of the outward and inward solutions at R_M does not guarantee that the total solution will be zero at $r = R$. Therefore, we perform an additional iteration procedure, in which the eigenvalue β_n is changed by a small amount until the value at R is satisfactory small ($S_n^{out}(R) < \epsilon$). We define a parameter

$$\mu_n = 100\mathfrak{Re}(\beta_n\epsilon), \qquad (41)$$

and for every iteration step we decrease its value by a half, changing the eigenvalue

$$\beta_n \leftarrow \beta_n(1 \pm \mu_n) \qquad (42)$$

where the sign is determined in the following way:

1) sign = 1.
2) If $\mathfrak{Re}(\beta_n)\mathfrak{Re}(S_n^{out}(R) - S_n(R)) < 0$ then sign = −1.
3) If $\frac{dS_n^{out}}{dr}|_R > 0$ then sign = − sign.

It means that first, the sign is calculated as the sign of the product $\mathfrak{Re}(\beta_n)$ times $\mathfrak{Re}(S_n^{out}(R) - S_n(R))$, where $S_n(R)$ is the value of the asymptotic function at R, given in Eq. (39) and $S_n^{out}(R)$ is the value of the outward integrated function at the same point. Then, we test the shape of derivative of $S_n^{out}(R)$. If the outward function is an increasing function, we invert the previous calculated sign.

4. Results

4.1. Bound levels

We will start to illustrate the results produced by our computational methods for bound state cases, where the energy parameter E is negative. In all the following examples we use $l = 0$ without loss of generality. Let us analyze the Coulombian case in which $E = -2.0$ a.u., because it results in analytic integer charges.

Fig. 1 displays the first 20 functions corresponding to the case of a Coulombian auxiliary potential

$$U(r) = -\frac{Z}{r} \qquad (43)$$

where $Z = 0$, and a Yukawa auxiliary potential

$$V(r) = -\frac{e^{-\alpha r}}{r} \qquad (44)$$

with $\alpha = 0$. Therefore, the Schrödinger equation (1) leads to

$$\left[-\frac{1}{2}\frac{d^2}{dr^2} - E\right]S_n(r) = -\beta_n\left(-\frac{1}{r}\right)S_n(r). \qquad (45)$$

Hence, the Sturmian functions S_n become the bound solutions of the Schrödinger equation

$$\left[-\frac{1}{2}\frac{d^2}{dr^2} - \beta_n\left(\frac{1}{r}\right)\right]S_n(r) = ES_n(r) \qquad (46)$$

for a charge $Z = \beta_n$ and a negative energy E.

The figure illustrates the main features of the Coulomb Sturmian functions, i.e., they are concentrated in a desired spatial region, according to the assigned energy parameter. The maximum value of the functions are located at a position roughly proportional to n, and the functions are completely different at low r
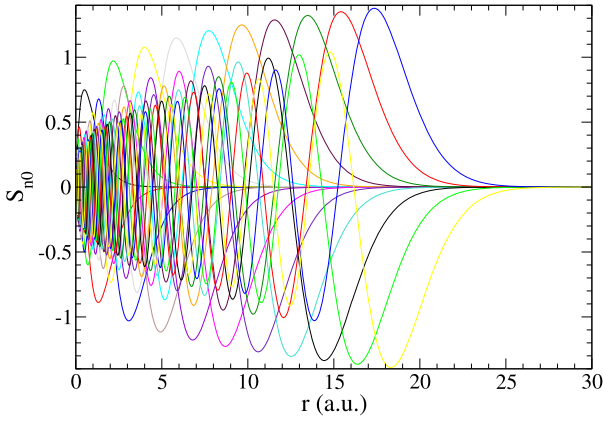
Fig. 1. First Sturmian functions S_{n0} for an auxiliary potential $U(r) = 0$, a generating potential $V(r) = -1/r$, and an energy $E = -2.0$ a.u.

Table 1
Eigenvalues β_n corresponding to the eigenfunctions displayed in Fig. 1. The parameters used are $N = 15\,000$, $R = 15$ a.u., and $\epsilon = 10^{-19}$.

n	β_n (a.u.) (from tridiagonalization)	β_n (a.u.) (iterated)
1	2.0000010000036230	2.0000000000000004
2	4.0000020000378882	4.0000000000000027
3	6.0000030000019908	5.9999999999999991
4	8.0000039999879586	8.0000000000000000
5	10.000005000006629	10.000000000000000
6	12.000006000016795	11.999999999999998
7	14.000007000851765	14.000000000000000
8	16.000008036012492	15.999999999999998
9	18.000010008979984	18.000000000000004
10	20.000029747422087	20.000000000000007
11	22.000282563822449	21.999999999999989
12	24.002623323374774	23.999999999999996
13	26.017292717385022	26.000000000000011
14	28.077799058971706	27.999999999999996
15	30.244131003759417	30.000000000000014
16	32.572306361097951	32.000000000000007
17	35.088636277394251	34.000000000000014
18	37.796936652335653	36.000000000000014
19	40.693198062114490	38.000000000000014
20	43.772489603945814	40.000000000000007

Table 2
Convergence of the fourth Sturmian function $S_{nl} = S_{40}$, for an auxiliary potential $U(r) = 0$, a generating potential $V(r) = -1/r$, and an energy $E = -2.0$ a.u. The parameters used are $N = 500$, $R = 10$ a.u., and $\epsilon = 10^{-12}$.

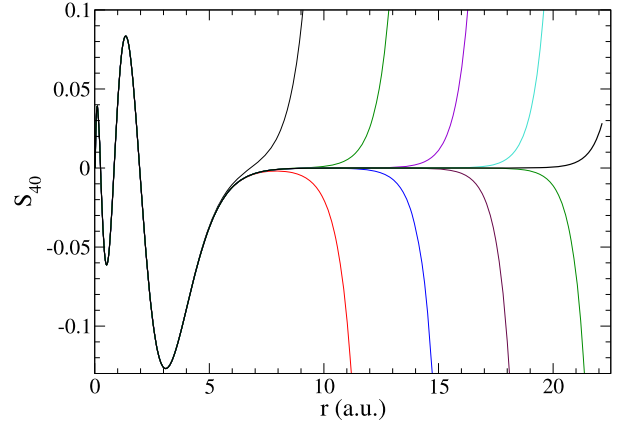| Iteration step	β_4 (a.u.)	$\Delta\eta_4$	$\Delta\beta_4$ (a.u.)
1	8.00159998727414	−9.326E−03	−1.681E−03
2	7.99991860322833	4.667E−04	8.582E−05
3	8.00000441966577	−2.566E−05	−4.659E−06
4	7.99999976082981	1.372E−06	2.522E−07
5	8.00000001300532	−7.520E−08	−1.365E−08
6	7.99999999935320	4.021E−09	7.391E−10
7	8.00000000009229	−2.204E−10	−4.002E−11
8	8.00000000005227	1.197E−11	2.172E−12
9	8.00000000005444	−6.482E−13	−1.177E−13

Fig. 2. Convergence of the fourth Sturmian function $S_{nl} = S_{40}$ for an auxiliary potential $U(r) = 0$, a generating potential $V(r) = -1/r$, and an energy $E = -2.0$ a.u. The curves correspond to the first iteration steps displayed in Table 2.

values. Hydrogenic functions, on the other hand, have the same shape at low r, and are spread around a wide spatial range. The last maximum of the hydrogenic function ($H_{n,l} = H_{20,0}$) is located at $r \approx 700$ a.u. Its corresponding CSF function is the last wave displayed here ($S_{n,l} = S_{20,0}$), whose maximum is located at $r \approx 18$ a.u.

For the Schrödinger equation (46) with $E = -2$ a.u., the charges are even integer values $\beta_n = 2n$. The resulting β_n from the tridiagonalization routine are given in the second column of Table 1, where it can be seen that the routine provides an accuracy of 10^{-5} for the lower charges, but misses many of the higher eigenvalues. We used a numerical grid having $N = 15\,000$ points, and with the boundary condition $C_N = e^{-k\Delta r}$ imposed at $R = 15$ a.u. This R value is too low for the higher functions, specially for those with $n > 15$, where the asymptotic decaying condition is reached for $r > 15$ a.u. That is the main reason for the accuracy problems at the higher eigenvalues. We applied the correction algorithm explained in Section 3.5, and displayed the results in the third column of the table. With relatively very low computation resources, we can obtain all the eigenvalues with more than 15 significant figures.

In order to illustrate how the iterative algorithm works, we show the convergence of the eigenvalues corresponding to the fourth function $S_{nl} = S_{40}$. We show in Table 2 the partial results for the successive iteration steps, starting the procedure from the

eigenvalue given by the tridiagonalization routine. In order to appreciate the convergence, we display the differences in the logarithmic derivatives $\Delta\eta_4 = \eta_4^{\text{inw}} - \eta_4^{\text{out}}$, and the correction factor $\Delta\beta_n$ given by the formula (B.10). It is important to note that the results displayed in this table were obtained with a much coarser grid having $N = 500$ points, otherwise, it would not be easy to appreciate the power of the iterative correction method.

Although every successive iteration step changes the eigenvalue function at a larger significant figure, it has a dramatic effect in the corresponding eigenfunction. Since the numerical solution is a mixture of a bound decreasing solution with a small component of a divergent function, we can always find a large r point at which the divergent part becomes dominant. However, our iterative method sets this point away in a very effective way, as is shown in Fig. 2.

4.2. Outgoing boundary conditions

As an example of outgoing boundary conditions, we calculate the case in which there is a free auxiliary potential $U(r) = 0$ and the generating potential is a Hulthén potential

$$V(r) = -\frac{e^{(-r/\alpha)}}{(1 - e^{(-r/\alpha)})}. \tag{47}$$

This potential has analytical solutions, where the eigenvalues are

$$\beta_n = \frac{n(n - 2i\sqrt{(2E)}\alpha)}{2\alpha^2}. \tag{48}$$

The result of the first 15 eigenfunctions are displayed in Fig. 3 (both the real and imaginary part of the functions), for an energy

value $E = 0.6$ a.u., and a parameter $\alpha = 1.5$. The first tridiagonalization is performed imposing the outgoing boundary conditions at $R = 15$ a.u. At this value we also assigned the arbitrary normalization $S_n(R) = 1 + i0$. As shown in the figure, this is a good choice for the R value since the asymptotic boundary condition is already reached at $r \geqslant 10$ a.u. For the corrective iterations, the asymptotic outgoing boundary conditions are imposed at $R_a = R + 4\lambda$, where $\lambda = 2\pi/k$. From this point we start the inward integration, matching the logarithmic derivative at $R_m = R/2 = 7.5$ a.u. We do not show here the analytical results, since they are indistinguishable from our numerical calculations.

The numerical results of the eigenvalues are compared with the analytical values (48) in Table 3. The results show once more an excellent agreement with the analytical values, and we can generate even better results by giving a larger R value. As was pointed out in Section 3.2, there is a serious limitation in the standard diagonalization methods, for the maximum R value (since we need to invert the generating potential in the procedure of the matrix construction). Using our computational method, we are able to impose the outgoing boundary conditions at much further places, in which the generating potential is practically zero. For this particular calculation, we used $R_a = 15R = 225$ a.u.

The accuracy of these eigenvalues is of about 11 significant figures, and although this is an excellent achievement, it is lower than the accuracy obtained for the bound states.

The convergence power of the iterative algorithm is displayed in Table 4, where, again, we use a very coarse grid of $N = 100$ points, otherwise, the changes would not be perceptible. We display here the real part of the eigenvalues, and the relative discrepancies (in percent) between the logarithmic derivatives of the inward and outgoing integrations, and the correction factors.

Unlike the previous case, we will not illustrate the convergence of the functions corresponding to the eigenvalues displayed in Table 4 because they are too similar. In Fig. 4, we will, instead, show how similar are the continuum Sturmian functions, even for big changes in the eigenvalues. We calculated the functions corresponding to charges β_4 ranging from 2.8 to 4.0, which covers a range of $\pm 20\%$ of the analytic charge β_4. Although there are large differences between the charges, the functions are insensitive to them. That illustrates the huge effort needed in the adjusting procedure for continuum states, and explain the relatively low accuracy (compared to the bound states).

Table 4
Convergence of the fourth Sturmian function $S_{nl} = S_{40}$ iterations, for an auxiliary potential $U(r) = 0$, a generating Hulthén potential $V(r) = -\exp(-r/\alpha)/(1 - \exp(-r/\alpha))$, for $\alpha = 1.5$, an energy $E = 0.6$ a.u., and outgoing boundary conditions. The parameters used are $N = 100$, $R = 15$ a.u., and $\epsilon = 10^{-8}$.

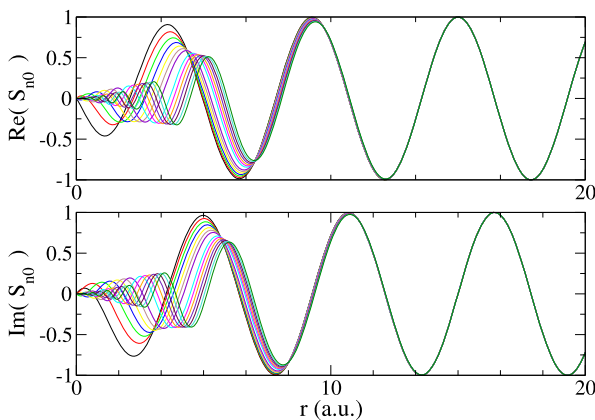| Iteration step	$\mathfrak{Re}(\beta_4)$ (a.u.)	$|\Delta\eta_4|$ (%)	$|\Delta\beta_4|$ (a.u.)
1	3.4635190	9.742E−04	0.287
2	3.5167349	1.125E−04	5.552E−02
3	3.5687958	3.592E−05	1.711E−02
4	3.5517540	1.021E−05	4.876E−03
5	3.5566216	2.939E−06	1.405E−03
6	3.5552604	8.461E−07	4.041E−04
7	3.5556279	2.432E−07	1.162E−04
8	3.5555328	6.998E−08	3.343E−05
9	3.5555562	2.013E−08	9.613E−06
10	3.5555508	5.789E−09	2.765E−06

Fig. 3. First Sturmian functions S_{n0} for an auxiliary potential $U(r) = 0$, a generating Hulthén potential $V(r) = -\exp(-r/\alpha)/(1 - \exp(-r/\alpha))$, for $\alpha = 1.5$, an energy $E = 0.6$ a.u., and outgoing boundary conditions.
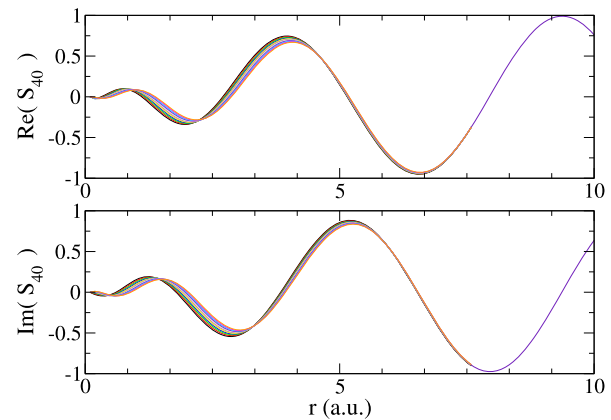

Fig. 4. Convergence of the fourth Sturmian function $S_{nl} = S_{40}$, for an auxiliary potential $U(r) = 0$, a generating Hulthén potential $V(r) = -\exp(-r/\alpha)/(1 - \exp(-r/\alpha))$, for $\alpha = 1.5$, and an energy $E = 0.6$ a.u. The curves correspond to different eigenvalues in the range $\pm 20\%$ of β_4.

Table 3
Eigenvalues β_n corresponding to the eigenfunctions displayed in Fig. 3. The parameters used are $N = 15\,000$, $R = 15$ a.u., and $\epsilon = 10^{-19}$.

n	β_n (a.u.) (iterated)	Analytic
1	(0.22222222222228, −0.73029674333998)	(0.22222222222222, −0.73029674334022)
2	(0.88888888889177, −1.46059348668004)	(0.88888888888889, −1.46059348668044)
3	(1.99999999999392, −2.19089023003007)	(2.00000000000000, −2.19089023002066)
4	(3.55555555555657, −2.92118697334976)	(3.55555555555556, −2.92118697336088)
5	(5.55555555558341, −3.65148371663824)	(5.55555555555556, −3.65148371670111)
6	(8.00000000003550, −4.38178046004462)	(8.00000000000000, −4.38178046004133)
7	(10.8888888889295, −5.11207720336655)	(10.8888888888889, −5.11207720338155)
8	(14.2222222221204, −5.84237394677867)	(14.2222222222222, −5.84237394672177)
9	(17.9999999998399, −6.57267068992702)	(18.0000000000000, −6.57267069006199)
10	(22.2222222221056, −7.30296743330756)	(22.2222222222222, −7.30296743340221)
11	(26.8888888886373, −8.03326417677695)	(26.8888888888889, −8.03326417674244)
12	(31.9999999993362, −8.76356092011071)	(32.0000000000000, −8.76356092008266)
13	(37.5555555557964, −9.49385766323422)	(37.5555555555556, −9.49385766342288)

Table 5

Convergence of the fourth Sturmian function $S_{nl} = S_{40}$ iterations, for an auxiliary potential $U(r) = \frac{-Z}{r}$, a generating Yukawa potential $V(r) = -\exp(-\alpha r)/r$, for $\alpha = 0.01$, an energy $E = 2.0$ a.u. and box boundary conditions. The parameters used are $N = 1300$, $R = 10$ a.u., and $\epsilon = 10^{-15}$. First iteration steps.

Iteration step	β_4 (a.u.)	$\|\Delta\eta_4\|$ (%)	$\|\Delta\beta_4\|$ (a.u.)	$S_{40}(R)$
1	3.3744134052266594	3.292E−02	1.027E−02	1.628E−02
2	3.3846881810737082	6.025E−03	1.923E−03	2.980E−03
3	3.3866110480548040	1.073E−03	3.437E−04	5.304E−04
4	3.3869547507530382	1.900E−04	6.091E−05	9.393E−05
5	3.3870156623370371	3.361E−05	1.078E−05	1.662E−05
6	3.3870264407058168	5.946E−06	1.907E−06	2.940E−06
7	3.3870283474330174	1.052E−06	3.373E−07	5.201E−07
8	3.3870286847228628	1.860E−07	5.966E−08	9.200E−08
9	3.3870287443871274	3.291E−08	1.055E−08	1.628E−08
10	3.3870287549413121	5.822E−09	1.867E−09	2.883E−09
11	3.3870287568082702	1.030E−09	3.303E−10	5.132E−10
12	3.3870287571385220	1.822E−10	5.842E−11	9.406E−11
13	3.3870287571969437	3.222E−11	1.033E−11	1.991E−11
14	3.3870287572072759	5.704E−12	1.829E−12	6.799E−12
15	3.3870287572091051	1.000E−12	3.208E−13	4.473E−12
16	3.3870287572094258	1.906E−13	6.111E−14	4.072E−12
17	3.3870287572094870	2.274E−14	7.291E−15	3.989E−12
18	3.3870287572094941	6.473E−15	2.076E−15	3.981E−12
19	3.3870287572094964	5.684E−15	1.823E−15	3.981E−12
20	3.3870287572094981	1.263E−15	4.051E−16	3.979E−12

Table 6

Second iteration steps, corresponding to the basis calculated in Table 5.

Iteration step	β_4 (a.u.)	$S_{40}(R)$
1	3.3870287572094981	3.979E−12
2	3.3870287572106452	2.522E−12
3	3.3870287572117923	1.070E−12
4	3.3870287572129394	−3.919E−13
5	3.3870287572123656	3.365E−13
6	3.3870287572129394	−3.919E−13
7	3.3870287572126525	−2.749E−14
8	3.3870287572125091	1.545E−13
9	3.3870287572126525	−2.749E−14
10	3.3870287572125810	6.394E−14
11	3.3870287572126525	−2.749E−14
12	3.3870287572126165	1.832E−14
13	3.3870287572126525	−2.749E−14
14	3.3870287572126347	−1.691E−15
15	3.3870287572126259	4.626E−15
16	3.3870287572126347	−1.691E−15
17	3.3870287572126303	1.565E−15
18	3.3870287572126347	−1.691E−15
19	3.3870287572126325	−6.530E−16

4.3. Box boundary conditions

The box boundary conditions $S_{nl}(0) = S_{nl}(R) = 0$ have been imposed on the example below. This is a case of a Coulombian auxiliary potential $U(r) = \frac{-Z}{r}$ for $Z = 1$, and a generating Yukawa potential $V(r) = -\exp(-\alpha r)/r$, for $\alpha = 0.01$. As explained in Section 3.5.3, the stationary boundary condition requires a first group of iteration steps in which the logarithmic derivatives are matched at a certain point located beyond the box limit $R_M = R + \frac{\lambda}{8}$. We set the box limit at $R = 10$ a.u., and the parameter $E = 2.0$ a.u. Table 5 shows the convergence of the 4th function iterations, starting from the initial value given by the tridiagonalization routine, until the differences in the logarithmic derivatives fulfill the convergence criterion $\|\Delta\eta_n\| < \epsilon = 10^{-15}$. The last column of the Table shows the value of the function at the point $r = R$, and although is decreasing through the iterations, it is not null.

Once the first iteration converged, we started a second type of iterations where the eigenvalue β_n is finely adjusted, in order to annihilate the value of the wavefunction at the boundary R, according to the procedure explained in Section 3.5.3. The results of the second iteration steps are displayed in Table 6.

4.4. Outgoing boundary conditions with complex energies

As an example of a Sturmian basis set with outgoing boundary conditions and complex energies (complex rotation), we present the case of a Coulomb auxiliary potential $U(r) = -\frac{1}{r}$, and a generating Yukawa potential $V(r) = -\frac{e^{-\alpha r}}{r}$, for $\alpha = 0.1$, and $l = 1$. In part (a) of Fig. 5 the real part of the first 5 functions are displayed for a positive energy $E = 2.0$ a.u., and with outgoing waves boundary condition imposed at $R = 40$ a.u. The auxiliary Coulomb potential produces solutions with an asymptotic behavior

$$\lim_{r \to \infty} S_{nl} \propto e^{-ikr + i\frac{Z}{k}\ln(2kr)}. \tag{49}$$

As seen in the figure and explained in Section 2, this oscillatory behavior is the same for all the basis functions, and for positive energies, it does not diverge.

With the complex rotation, the purely outgoing waves vanish as the electron coordinate goes to infinity, exactly like a bound state. All continuum–continuum integrals are treated as a L^2 integrable case. We rotate the wavenumber k an angle θ_k, defined as
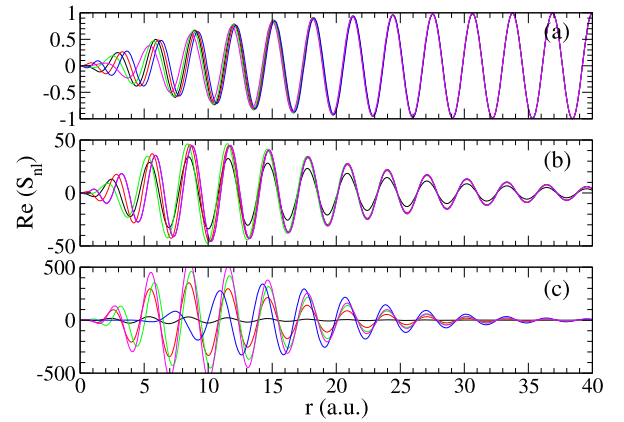

Fig. 5. Real part of the first 5 Sturmian functions S_{n1}, for an auxiliary Coulomb potential $U(r) = -\frac{1}{r}$, a generating Yukawa potential $V(r) = -\frac{e^{-\alpha r}}{r}$, for $\alpha = 0.1$ and with outgoing waves boundary conditions. (a) Positive energy $E = 2.0$ a.u., corresponding to a wavenumber $k = 2.0$ a.u. (b) Complex energy $E = 1.9962 + i0.17464$ a.u., corresponding to a wavenumber $k_r = 2.0$ a.u., rotated an angle $\theta_k = 2.5°$. (c) Complex energy $E = 1.9847 + i0.70531$ a.u., corresponding to a wavenumber $k_r = 2.0$ a.u., rotated an angle $\theta_k = 5°$.

$$k = \frac{k_r}{\cos(\theta_k)} e^{i\theta_k}. \tag{50}$$

Using this definition, the real part of the wavenumber (k_r) is always the same, regardless of the angle of rotation. The energy parameter E is calculated from this definition as

$$E = \frac{E_r}{\cos^2(\theta_k)} e^{i\theta_E} \tag{51}$$

where $\theta_E = 2\theta_k$, and the real part of the energy is defined as

$$E_r = \frac{k_r^2}{2}. \tag{52}$$

We illustrate how the complex rotation works in Fig. 5, where in part (b) the energy is rotated 5° (i.e., $\theta_k = 2.5°$), and in part (c) $\theta_k = 5°$. In these cases the outgoing boundary conditions are imposed at $R = 40$ a.u. The functions shown in the figure are normalized with the same conditions as the bound levels, determined in Eq. (36).

5. Conclusions

In this work, we presented an efficient recipe to numerically generate a Generalized Sturmian basis set, defined for any kind

of generating and auxiliary potentials; and for negative, positive and complex energies. A complete discussion on how to impose the appropriate boundary conditions and a detailed description of the algorithms utilized are also provided. This complements our previous publications [17,18,20,22], where we presented the basic fundamentals of the theory and illustrated the use of this kind of basis set in atomic scattering applications.

The starting point of the construction is the generation of the charge eigenvalues by discretizing the Sturmian equation in a uniform grid. This transforms the problem into a finite-difference recurrence relation. The boundary conditions at the origin and at large distances—on the configuration space—required to define a Sturm–Liouville problem, are imposed on the recurrence relation. In all our applications we use regular wavefunctions which set the boundary condition at the origin. Asymptotically, we developed a method to allow a standing—an incoming—or an outgoing-wave behavior for positive-energy Sturmian functions. Those boundary conditions are applied by including a modification in the last diagonal elements of the Hamiltonian matrices. The same conditions can be imposed to complex-energy functions, taking into account that the rotation in the complex plane implies an exponential decrease of the functions, at large distances.

For standing-wave boundary conditions, and also for negative-energy functions, the Hamiltonian matrices are real and, in general, standard numerical routines can be employed. However, for positive energies and incoming—or outgoing—wave behaviors, the eigenvalue method employed must be able to deal with complex matrices. For these cases we developed a fast and accurate algorithm for obtaining the eigenvalues of a tri-diagonal complex matrix. This method is based on an implicit QR method with the Wilkinson shift, explained by Luk and S. Qiao [24]. Although this method may, in principle, also generate the Sturmian eigenvectors, it fails when the numerical grid includes spatial regions in which the generating potential is too low.

For that reason, we introduced another iterative algorithm that allows to obtain, very fast, very accurate eigenvalues and eigenvectors. In this approach, eigenvalues are obtained by the QR method first, and then they are used as a pre-conditioner for a further predictor–corrector procedure. The method includes a numerical outwards integration from the origin to a given matching point, followed by an inwards integration from the asymptotic region towards the origin. At the matching point the logarithmic derivatives are calculated for both solutions, and iterations are performed until both of them coincide. A careful selection of the matching point is also needed to achieve excellent convergence properties in the eigenvalues and eigenvectors.

In this paper we showed that the method implemented is highly efficient for negative, positive, and even complex energies. This is proven by comparing the eigenvalues derived with the theoretical results, for some cases in which the Sturmian equation can be solved analytically.

Acknowledgements

Appendix A. Description of the procedure for eigenvalues calculation

In this appendix, we describe briefly the main steps used in our QR algorithm, for the diagonalization of a complex-symmetric tri-diagonal matrix $\mathbf{A}$ of size $N \times N$. The elements of this matrix are denoted d_i and e_i, for the diagonal and off-diagonal elements, respectively.

1. Starting from the last eigenvalue N
   (a) loop for $n = N$ to 1
      i. Construct the trailing matrix $\mathbf{L^{(n-1)}}$, which is the last 2×2 principal sub-matrix of $\mathbf{A}$

$$\mathbf{L^{(N-1)}} = \begin{pmatrix} A_{n-1,n-1} & A_{n-1,n} \\ A_{n,n-1} & A_{n,n} \end{pmatrix}. \tag{A.1}$$

      ii. Diagonalize $\mathbf{L^{(n-1)}}$ and select μ, the eigenvalue closer to $\mathbf{A}_{n,n}$.
      iii. Determine $x_1 = d_1 - \mu$, and $x_2 = e_1$.
      iv. Loop for $j = 1$ to $N - 1$
         A. Construct a reduced 2×2 principal sub-matrix of $\mathbf{A}$

$$\mathbf{L^{(j)}} = \begin{pmatrix} A_{j,j} & A_{j+1,j} \\ A_{j+1,j} & A_{j+1,j+1} \end{pmatrix}. \tag{A.2}$$

         B. Construct the transformation matrix $\mathbf{G^{(j)}}$ (Eq. (26)) and its transpose $(\mathbf{G^{(j)}})^T$ in the following way:

         if $\left(|x_1| > |x_2|\right)$ **then**
         $$t \equiv \frac{x_2}{x_1}; \qquad c_j \equiv \frac{1}{\sqrt{1+t^2}}; \qquad s_j \equiv t.c$$
         else
         $$t \equiv \frac{x_1}{x_2}; \qquad s_j \equiv \frac{1}{\sqrt{1+t^2}}; \qquad c_j \equiv t.s$$
         endif.

         C. Perform the transformation

$$\mathbf{L^{(j)}} \leftarrow \mathbf{G^{(j)}} \mathbf{L^{(j)}} \mathbf{G^{j}}^T. \tag{A.3}$$

         D. From the new values of $\mathbf{L^{(j)}}$, reconstruct the new matrix $\mathbf{A^{(j+1)}}$ with

$$\begin{aligned} \mathbf{A}_{j,j}^{(j+1)} &= \mathbf{L}_{1,1}^{(j)}; & \mathbf{A}_{j,j+1}^{(j+1)} &= \mathbf{L}_{1,2}^{(j)}; \\ \mathbf{A}_{j+1,j}^{(j+1)} &= \mathbf{L}_{2,1}^{(j)}; & \mathbf{A}_{j+1,j+1}^{(j+1)} &= \mathbf{L}_{2,2}^{(j)} \end{aligned} \tag{A.4}$$

         and

$$\begin{aligned} \mathbf{A}_{j+2,j}^{(j+1)} &= c_j \mathbf{A}_{j+1,j}^{(j)} + s_j \mathbf{A}_{j+1,j+2}^{(j)}; \\ \mathbf{A}_{j+2,j+1}^{(j+1)} &= c_j \mathbf{A}_{j+1,j+1}^{(j)}. \end{aligned} \tag{A.5}$$

         E. Redefine x_1 and x_2 in the following way

$$\begin{aligned} x_1 &= \mathbf{A}_{j,j-1}^{(j+1)}, \\ x_2 &= s_j \mathbf{A}_{j+1,j+2}^{(j)}. \end{aligned} \tag{A.6}$$

         F. Reassign

$$\begin{aligned} d_i &= \mathbf{A}_{j,j}^{(j+1)}, \\ e_i &= \mathbf{A}_{j,j+1}^{(j+1)}. \end{aligned} \tag{A.7}$$

         G. End of the loop (1(a)iv).
      v. Check convergence (27) of the off-diagonal element e_N.
      vi. If convergence is not achieved, go back to (1(a)i).
   (b) Set $n = (N - 1)$ and continue the loop (1a).
2. Perform a selection of the eigenvalues (keep only those that are within the desired range).
3. Sort the eigenvalues.

Appendix B. Correction formula for eigenvalue calculation

At any step of the iteration outlined in Section 3.5, an outward integration is carried out from the origin to a matching point (for bound states it is r_t), and an inward integration from r_∞ to r_t. The results of these two integrations are written as S_n^{out} and S_n^{inw}. The degree of mismatch between both functions, as measured by the difference between the logarithm derivatives η_n of these functions, is used to estimate an improved trial eigenvalue. In the present appendix, we will explain how to calculate the increment $\Delta\beta_n$, needed to replace each eigenvalue β_n by

$$\beta_n \leftarrow \beta_n + \Delta\beta_n. \tag{B.1}$$

If we let $P_1(r)$ and $Q_1(r)$ represent the radial wave function $S_n(r)$ and its derivative for the eigenvalue β_n^1, and let $P_2(r)$ and $Q_2(r)$ represent the same two quantities for β_n^2, then the Generalized Sturmian radial equation (1) is written for any case as

$$-\frac{1}{2}\frac{dQ_1}{dr} + \frac{l(l+1)}{2r^2}P_1(r) + U(r)P_1(r) - EP_1(r)$$
$$= -\beta_n^1 V(r)P_1(r), \tag{B.2}$$
$$-\frac{1}{2}\frac{dQ_2}{dr} + \frac{l(l+1)}{2r^2}P_2(r) + U(r)P_2(r) - EP_2(r)$$
$$= -\beta_n^2 V(r)P_2(r). \tag{B.3}$$

Multiplying Eq. (B.2) by P_2 and Eq. (B.3) by P_1, and subtracting, it follows that

$$-\frac{1}{2}\left(\frac{dQ_1}{dr}P_2 - \frac{dQ_2}{dr}P_1\right) = -\left(\beta_n^1 - \beta_n^2\right)P_1 V P_2. \tag{B.4}$$

The left side of Eq. (B.4) is

$$-\frac{1}{2}\left(\frac{dQ_1}{dr}P_2 - \frac{dQ_2}{dr}P_1\right) = -\frac{1}{2}\frac{d}{dr}(Q_1 P_2 - Q_2 P_1), \tag{B.5}$$

so,

$$\frac{d}{dr}(Q_1 P_2 - Q_2 P_1) = 2\left(\beta_n^1 - \beta_n^2\right)P_1 V P_2. \tag{B.6}$$

We integrate Eq. (B.6) from $r = 0$ to $r = \infty$, in two steps. First, using the outward functions P_1^{out} and P_2^{out} from $r = 0$ to the matching point $r = r_t$, and then, using the inward functions P_1^{inw} and P_2^{inw} from $r = \infty$ to $r = r_t$. Taking into account that we are seeking regular solutions (Eq. (2)) and with the same asymptotic conditions, the integration resumes as

$$\left(Q_2^{\text{out}}P_1^{\text{out}} - Q_1^{\text{out}}P_2^{\text{out}}\right)\big|_{r_t} - \left(Q_2^{\text{inw}}P_1^{\text{inw}} - Q_1^{\text{inw}}P_2^{\text{inw}}\right)\big|_{r_t}$$
$$= 2\left(\beta_n^2 - \beta_n^1\right)\left[\int_0^{r_t} P_1^{\text{out}}V P_2^{\text{out}} + \int_{r_t}^{\infty} P_1^{\text{inw}}V P_2^{\text{inw}}\right]. \tag{B.7}$$

If we demand that the functions $P_j^{\text{out}}(r_t) = P_j^{\text{inw}}(r_t)$ for $j = 1, 2$ and assuming that β_n^2 is the exact eigenvalue and $P_2(r)$ is the exact eigenvector (and, hence, $Q_2^{\text{out}}(r_t) = Q_2^{\text{inw}}(r_t)$), then

$$P_2(r_t)\left(Q_1^{\text{inw}}(r_t) - Q_1^{\text{out}}(r_t)\right) = 2\left(\beta_n^2 - \beta_n^1\right)\int_0^{\infty} P_1 V P_2. \tag{B.8}$$

Since we assumed that P_2 is exact, the correction to the calculated eigenvalue must fulfill

$$\beta_n^1 + \Delta\beta_n = \beta_n^2. \tag{B.9}$$

Replacing the result given in (B.8), we obtain

$$\Delta\beta_n = \frac{S_n(r_t)\left(\frac{dS_n^{\text{inw}}}{dr} - \frac{dS_n^{\text{out}}}{dr}\right)\big|_{r=r_t}}{2\left(\int_0^{r_t} S_n^{\text{out}}(r)V(r)S_n^{\text{out}}(r) + \int_{r_t}^{\infty} S_n^{\text{inw}}(r)V(r)S_n^{\text{inw}}(r)\right)}. \tag{B.10}$$

References

[1] H. Shull, P.O. Löwdin, J. Chem. Phys. 30 (1959) 617.
[2] M. Rotenberg, Ann. Phys. 19 (1962) 262.
[3] M. Rotenberg, Adv. At. Mol. Phys. 6 (1970) 233.
[4] W. Glöckle, J. Hüfner, H.A. Weidenmuller, Nuc. Phys. A 90 (1967) 481.
[5] O. Goscinski, Preliminary research report no. 217, Quantum Chemistry Group, Uppsala University, 1968 (Originally unpublished). Included as an appendix in: Adv. Quant. Chem. 41 (2003) 51.
[6] J. Avery, J. Avery, O. Goscinski, Natural orbitals from generalized Sturmian calculations, Adv. Quant. Chem. 43 (2003) 207.
[7] J. Avery, J. Avery, Generalized Sturmians and Atomic Spectra, World Scientific, Singapore, 2006.
[8] E. Holøien, Phys. Rev. 104 (1956) 1301.
[9] M.W.J. Bromley, J. Mitroy, Int. J. Quant. Chem. 107 (2007) 1150.
[10] R. Szmytkowski, J. Phys. A 31 (1998) 4963.
[11] G. Gasaneo, F.D. Colavecchia, J. Phys. A 36 (2003) 8443.
[12] E. Foumouo, G.L. Kamta, G. Edah, B. Piraux, Phys. Rev. A 74 (2006) 063409.
[13] J.M. Ngoko Djiokap, E. Foumouo, M.G. Kwato Njock, X. Urbain, B. Piraux, Phys. Rev. A 81 (2010) 042712.
[14] G. Rawitscher, Phys. Rev. C 25 (1982) 2196.
[15] J.H. Macek, S.Yu. Ovchinnikov, Phys. Rev. A 54 (1996) 544.
[16] S.Yu. Ovchinnikov, J.H. Macek, Phys. Rev. A 55 (1997) 3605.
[17] J.M. Randazzo, A.L. Frapiccini, F.D. Colavecchia, G. Gasaneo, Phys. Rev. A 79 (2009) 022507.
[18] J.M. Randazzo, A.L. Frapiccini, F.D. Colavecchia, G. Gasaneo, Int. J. Quant. Chem. 109 (2009) 125.
[19] J.M. Randazzo, Métodos ab-initio para el problema de tres cuerpos con interacciones Coulombianas, PhD thesis, Instituto Balseiro, Universidad Nacional de Cuyo, Argentina, 2009.
[20] J.M. Randazzo, L.U. Ancarani, G. Gasaneo, A.L. Frapiccini, F.D. Colavecchia, Phys. Rev. A 81 (2010) 042520.
[21] G. Gasaneo, L.U. Ancarani, Phys. Rev. A, submitted for publication.
[22] A.L. Frapiccini, J.M. Randazzo, G. Gasaneo, F.D. Colavecchia, J. Phys. B 43 (2010) 101001.
[23] J. Dongarra, et al., LAPACK Users' Guide, 3rd ed., SIAM, Philadelphia, USA, 1999.
[24] F.T. Luk, S. Qiao, Linear Algebra Appl. 316 (2000) 171.
[25] G.H. Golub, C.F. Van Loan, Matrix Computations, 3rd ed., Johns Hopkins University Press, Baltimore, USA, 1996.
[26] V. Hernández, J.E. Román, A. Tomás, V. Vidal, http://www.grycap.upv.es/slepc.
[27] W.R. Johnson, Atomic Structure Theory: Lectures on Atomic Physics, Springer-Verlag, Heidelberg, Germany, 2007.
[28] F. Salvat, J.M. Fernandez-Varea, W. Williamson Jr., Comp. Phys. Comm. 90 (1995) 151.